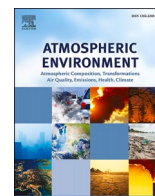


Contents lists available at [ScienceDirect](https://www.sciencedirect.com)

# Atmospheric Environment

journal homepage: <http://www.elsevier.com/locate/atmosenv>

## Determination of radiological background fields designated for inverse modelling during atypical low wind speed meteorological episode

Petr Pecha<sup>a,\*</sup>, Ondřej Tichý<sup>a</sup>, Emilie Pechová<sup>b</sup><sup>a</sup> Institute of Information Theory and Automation of the Czech Academy of Sciences, v.v.i., Pod Vodarenskou vezi 4, 182 08, Prague 8, Czech Republic<sup>b</sup> Institute of Nuclear Research, Rez near Prague, Subdivision EGP, Czech Republic

### ARTICLE INFO

#### Keywords:

Low wind speed  
 Atmospheric dispersion  
 Radioactivity dissemination  
 Inverse modelling  
 Hot spot occurrence

### ABSTRACT

This article focuses on the formation of complex trajectories of radiological background fields for atypical accidental discharges of radioactivity into the atmosphere during very low wind speed episodes (calms). Within several hours of a calm meteorological situation, a relatively significant level of radioactivity can be accumulated around the source. In the next stage, the calm situation is assumed to terminate and convective movement of the air immediately starts. A packet of accumulated radioactivity, which has the form of multiple Gaussian puffs, is drifted by wind. Consequently, the pollution is disseminated over the terrain. Significant transport of radioactivity even behind the protective zone of a nuclear facility (up to between 15 and 20 km) has been observed. Original optional statistical pre-processing of calm's results is inserted between the calm and convective stages of the trajectory generation which may improve performance of following computationally expensive methods of Bayesian filtering. Determination of complex trajectory passing through both calm and convective stages of the release scenario represents inevitable prior information for prospective assimilation techniques. Draft twin experiment is outlined for a simple assimilation scenario for re-estimation of the main model parameters based on a notional monitoring network in the outer convective region.

### 1. Introduction

A deterministic mathematical model always remains a mere simplification of complex physical phenomena; and a significant extent of uncertainties involved can degrade the credibility of the model predictions. The models only approximate the complicated real situation during an accidental radioactive release, e.g., (Drécourt, 2004; Evangelidou et al., 2017). Conventional analyses are based on a certain deterministic single set of input model parameters derived from the “best estimate” or conservative “worst case” choices. Deterministic calculations do not comply with the inherent uncertain character of the problem. Uncertainties related to imperfections of both the conceptual model and the computational schemes are involved (Korsakissok et al., 2020). Limited information may be available on the exact location or time of the release, quantities of materials emitted, dispersal mechanisms, or other source characteristics (Tichý et al., 2018). Nevertheless, experience accumulated in physical models of pollution propagation through the living environment provides valuable prior knowledge.

In consequence of inherent uncertainties, output radiological

quantities also have a random character; hence the processing and interpretation have to be based on the probabilistic basis. A stochastic character of the system calls for introduction of probabilistic-approach modelling with a possibility to define a measure of confidence in the model predictions. This approach allows us to proceed from the former deterministic calculations towards generation of probabilistic answers to assessment questions.

Simulation of uncertainty propagation through the model constitutes an inevitable tool for top-level modern modelling techniques designated as data assimilation, which can substantially improve the reliability of predictions (Carrassi et al., 2018). In reality, it represents a chain of consecutive steps starting with determination of the prior background fields of the system using a nominal set of all input parameters. Uncertainty and sensitivity analyses follow, which leads to the simulation of multiple random trajectories of pollution transport. Finally, a substantial benefit can result from the accessibility of the real measurements with noise incoming from terrain. The data assimilation procedure performs an optimal blending of all contending information resources, including the prior physical knowledge given by the model, observations

\* Corresponding author.

E-mail addresses: [pecha@utia.cas.cz](mailto:pecha@utia.cas.cz) (P. Pecha), [otichy@utia.cas.cz](mailto:otichy@utia.cas.cz) (O. Tichý), [emipe@seznam.cz](mailto:emipe@seznam.cz) (E. Pechová).

incoming from terrain, expert judgement, past experience and possibly also intuition. The data assimilation concept represents the true way from model to reality.

Furthermore, an inverse problem from the category of parameter estimation is examined when the system parameters (e.g., source term or short term predictions of the meteorological situation) are inferred from the experimental data. A comprehensive overview of the source term estimation methods is given in (Hutchinson et al., 2017). The importance of preliminary analysis of the background radiological fields is highlighted there. Optimisation approach and Bayesian-based probabilistic consideration techniques of Markov Chain Monte Carlo (MCMC), Sequential Monte Carlo (SMC<sup>1</sup>) and other efficient sampling methods are pointed out. The inverse problems are often improperly posed from the mathematical point of view due to information deficit. It is called an inverse problem because it starts with the results (the measured output of radiological quantities) and then infers the causes (refined model parameter values). This is the inverse of the original forward problem, which arises from the causes and then calculates the results. The inverse problem is highly non-linear and subjected to input data that is typically sporadic, noisy and sparse (Kabanikhin, 2008).

Recent progress includes consistent joint assimilation of the air sampling measurements and deposition observations (Winiarek et al., 2014), also taking into account the cumulated fallout measurements. An advance in this direction is represented by an introduction of the gamma dose rate (GDR<sup>2</sup>) measurement method aggregated with the most widespread measurement system (Saunier et al., 2013). The variable “ambient dose rate”  $D_{ambient}$  represents the sum of contributions of all gamma-emitting radionuclides  $n = 1, \dots, N$  according to:

$$D_{ambient} = \sum_{n=1}^{n=N} D_{plume}^n + \sum_{n=1}^{n=N} D_{deposit}^n \quad (1.1)$$

$D_{plume}^n$  resp.  $D_{deposit}^n$  stand for gamma dose rate from radionuclide  $n$  from air (plume) resp. from radioactivity deposited on the ground,  $N$  is total number of radionuclides in the release. This approach is based on the inverse problem solution described by the source-receptor equation techniques. The prior information is extracted from the fact that the main part of the dose rate signal corresponds to the few radionuclides. The respective contributions of the principal radionuclides are distinguished using only the information contained in the GDR measurements. The temporal evolution of the radioactive decay signal contains indirect information on the isotopic composition of the emissions. Some limits of the isotopic relationships can be roughly guessed from the core inventory and the type of the reactor damage. This method was validated on the Fukushima accident. Similarly, the emissions of two isotopes (noble gas <sup>133</sup>Xe and the aerosol-bound <sup>137</sup>Cs) into the atmosphere from the Fukushima Dai-ichi nuclear power plant accident were examined in (Stohl et al., 2012). The results of determination of the source term, atmospheric dispersion, and deposition are assembled. The first guess of the release rates is chosen based on fuel inventories and documented accident events at the site. This first guess is subsequently improved by inverse modelling. The source term reconstruction model is also implemented within the European nuclear emergency response system JRODOS (Kovalets et al., 2016; Schichtel, 2019). The source inversion is treated as a variational problem with an appropriately constructed cost function. The GDR measurements are taken at a wide range of distances from the source of pollution.

Capability and sensitivity levels of the European monitoring networks have been proved during some tiny radioactive releases on a European scale. In October 2017, most European countries reported unique atmospheric detections of the aerosol-bound ruthenium <sup>106</sup>Ru. Investigation of the unknown location and unknown magnitude of this

undeclared release took place in several institutions. The results are, e.g., reported in (Saunier et al., 2019; on the Czech national level Tichy et al., 2019). The source reconstruction methodology was based on the variational inverse modelling technique. Finally, forward simulation of the release from the most pertinent Mayak site (northern Ural region) consistently reproduced air concentrations in Europe. A similar episode of a rare low-level radionuclide discharge was the unusual accidental release of <sup>131</sup>I detected at several radionuclide monitoring stations in Central Europe in the fall of 2011. The unintended release was originally treated as a source of unknown location and unknown magnitude (Tichy et al., 2017). For the unknown release site, the inverse modelling was performed for many potential release sites and their likelihood was evaluated. After investigation, the IAEA was informed (IAEA, 2011) by Hungarian authorities that <sup>131</sup>I was released from the Institute of Isotopes in Budapest.

Finally, some additional activities at the national level are mentioned. The international cooperation in the area of the nuclear emergency management and population protection accomplished in the Institute of Information Theory and Automation (IITA) in Prague has a long tradition. Overall customisation of the former workstation version of the RODOS system (Real-time Online DecisiOn Support system) for the Czech territory has been accomplished. Scientific research related to the data assimilation topic and relevant models for radioactivity transport through the living environment is documented e.g. in (Hofman and Pecha, 2013) and mainly in the program product HARP<sup>3</sup> (HARP, 2010–2019).

Basic information on the existing and solved problems is given in a draft report (Šmídl et al., 2013). Suitability of the assimilation methods of recursive Bayesian filtering for modelling purposes is outlined. The Kalman filter procedure consisting of the data-update step and a consecutive time-update step is assessed. Bayesian approach to the data assimilation is based on representing the state uncertainty via a probability distribution. Each incoming measurement brings information about the ‘true’ state, reducing the original uncertainty. Radioactivity propagation is simulated on the basis of a recursive Bayesian-filtering procedure (Pecha et al., 2009). The lack of the actual measurements is compensated by artificial simulations (a twin experiment). The objective of this tracking is to recursively refine the model predictions on the basis of incoming measurements. A more efficient particle filter (PF<sup>4</sup>) solves the Bayesian update step for non-Gaussian probabilistic density function by empirically setting up an approximation of the posterior probability density. The particle filter numerically approximates the non-Gaussian posterior probability *pdf* using a set of particles  $x(i)$  (i.e., the random samples) of the state vector  $x$ , the set of measurements and importance weights.

Utilisation of the adaptive importance sampling in the context of the particle filtering and computational efficiency of the particle filter is examined in (Šmídl and Hofman, 2013). Several other PF applications have been resolved. As an example, an important scenario was treated in (Šmídl and Hofman, 2013a) where the sensors are carried on board of unmanned aerial vehicles (UAVs). Evaluation of the detection abilities of the monitoring networks is proposed in (Šmídl et al., 2014). A tuning-free method LS-APC for the linear inverse problem was examined in (Tichy et al., 2016). The LS-APC<sup>5</sup> algorithm is tested and compared with the standard methods using the data from the European Tracer Experiment (ETEX<sup>6</sup>). Advanced access to the source term estimation problem of multi-species atmospheric release based on the gamma dose rate measurements (GDR) is shown in (Tichy et al., 2018). The Bayesian methodology handles uncertain knowledge on the species ratios as well as the unknown temporal correlations of the source term. The prior

<sup>3</sup> Hazardous Radioactivity Propagation.

<sup>4</sup> Particle Filter.

<sup>5</sup> Least Squares with Adaptive Prior Covariance.

<sup>6</sup> European Tracer Experiment.

<sup>1</sup> Sequential Monte Carlo.

<sup>2</sup> Gamma dose rate.

knowledge of the ratios for different species is given in the form of bounds.

The assimilation to observation algorithm leads to a generalised least-square approach minimising a measure (proper cost function) of difference between the available information and the system state. Either advanced statistical assimilation procedures or a simpler optimisation approach (data assimilation as an optimisation task) can be classified as the proper methods of solution of the inverse problem. The inverse modelling for real-time estimation of the radiological consequences examined in (Pecha and Šmídl, 2016) adopts the recursive non-linear least-square minimisation. A twin experiment, generating noiseless simulated “artificial” observations, is studied to verify the minimisation algorithm. A sensitivity study of the measurement noise is included.

## 2. Extraction of the prior information from the dynamic model of the system

Data assimilation combines the prior knowledge information in the form of background fields with observations incoming from the terrain. The data assimilation problem is based on the Bayes theorem, where the posterior probability distribution is the probability distribution of the prior knowledge from numerical model multiplied by the probability distribution of the observations given each possible state of the model. A fast and sufficiently accurate algorithm is needed for generating the background fields of the radiological outputs. Feasibility of the modelling should be taken into account. For example, sequential Monte-Carlo assimilation methods require to recall many thousands of realisations of the system state trajectories. An equally important prerequisite is an adequate option of the mathematical-physical tool for the description of the actual release scenario. The commonly used dispersion models with appropriate modifications are usually assumed to provide the right basis for generating the background fields. However, certain complicated scenarios should be treated separately and the corresponding alternative algorithms have to be derived. Two of these situations have been encountered:

*Case CLOUD: Proposition of the fast scheme for generating 3-D external irradiation background fields from a radioactive cloud of a finite dimension drifted over the terrain.*

Advanced assimilation techniques coming from the sequential Monte-Carlo methods are computationally expensive and an effective procedure for fast simulation of the background fields of external irradiation has a crucial significance. A fast and sufficiently accurate approach to estimating the background cloudshine irradiation doses in 3-D was introduced in (Pecha and Pechová, 2014). A special decomposition of the Gaussian plume shape replaces the former rough estimations of semi-infinite cloud values. The substantial performance improvement increases the capability of the assimilation procedures and the respective recursive inverse techniques to run successively in the real-time mode. Special cases of such irradiation doses affecting for example a helicopter staff inside a plume can easily be assessed. Convergence of the finite cloud approximation to the tabulated semi-infinite cloud values for dose conversion factors is validated. The *Case CLOUD* could provide a proper tool for calculating the variable “ambient dose rate”  $D_{\text{ambient}}$  given by Eq. (1.1) representing the sum of contributions of all gamma-emitting radionuclides used for the gamma dose rate (GDR) measurements (Saunier et al., 2013).

*Case CALM: The background fields of the radiological output values for complicated scenarios of the radionuclide release at very low wind speed (calm) episodes.*

Recent research has been focused on designing effective computational techniques for comprehensive analysis of the potential risk connected with radioactivity propagation during calm meteorological situations (Lines et al. (2001), Lines and Deaves (1997)). A detailed description with an emphasis on further possible assimilation steps is introduced. The worst-case calm scenario is devised in several mutually

connected stages starting with a calm meteorological situation succeeded by wind:

- i. At the first stage, discharges of radionuclides into the motionless ambient atmosphere are assumed. During several hours of this calm meteorological situation, a relatively significant level of radioactivity can be accumulated around the source (cf. Section 3.2 for more details).
- ii. Statistical processing of the first-stage results follows. An original statistical method is designated, when estimating in advance the statistical properties of the radioactivity concentrations related just at the end of the calm episode  $T_{\text{END}}^{\text{CALM}}$ . Evidently non-Gaussian superposition of all partial Gaussian puffs  $m \in \{1, \dots, M\}$  can be substituted with only one representative equivalent Gaussian “superpuff” distribution (Section 4). Statistical derivation of the optimal approximant is outlined in (Kárný and Guy, 2012; Kárný and Pecha, 2020).
- iii. At the second stage, just after the calm termination, the convective movement of the air immediately starts. A pack of accumulated radioactivity in the form of multiple Gaussian puffs (or alternatively in a sole “superpuff”) is drifted by wind and pollution is disseminated over the terrain (Section 5).

The background trajectory is composed of a set of  $M$  discrete pulses simulating radioactive release into the motionless ambient when each partial pulse  $m \in \{1, \dots, M\}$  enters the convective transport separately. Alternatively, only one Gaussian “superpuff” proceeds onwards into the convection stage. Saving on computational load is evident, mainly over the implementation of more sophisticated dispersion models in connection with the assimilation algorithms.

## 3. Case CALM - low wind speed (calm) episode: release scenario, methodology and prior fields determination of an accidental release of radioactivity

### 3.1. Preliminary remarks on low wind speed meteorological situation

Terms such as „low wind speeds“ and „calm conditions“ are not defined precisely. Different authors may use such terms to imply different ranges of conditions and there is no generally accepted definition. The Beaufort Scale describes Force 0 as „calm“ and defines the equivalent wind speed at 10 m above ground as  $< 1$  knot ( $0.515 \text{ m s}^{-1}$ ). From different point of view, it can be meant as any wind speed below the starting threshold of the wind speed or direction sensors. It was found (Hyojoon et al., 2013), that the atmospheric dispersion factors were affected by the classification of wind intervals at a low wind speed of lower than  $2.0 \text{ m/s}$ . Horizontal wind oscillation starts. Steady-state Gaussian plume models start to be insufficient to account for the meander effect and some refinements have to be implemented. Hence, the wind speed of  $2.0 \text{ m s}^{-1}$  is commonly assumed as an upper limit of the low wind speed interval.

The regions of lowest wind speed are the low lying sheltered inland areas and this conditions varies significantly between different sites. Frequency of wind speeds and weather categories are determined by meteorological observations over a suitable period such as ten years. The percentage frequencies of hours, when the wind speeds at 10 m are based on data from 1981 to 1990 for selection of 6 inland sites (UK Meteorological Office), is shown in (Lines and Deaves, 1997). Wide differences between the sites are found here from 9.2 to 29.7% for  $u < 2 \text{ m s}^{-1}$  and from 0.6 to 6.6% for  $u < 0.5 \text{ m s}^{-1}$ . Similar statistics are presented in (Deaves and Lines, 1998) for selection of another 6 inland sites (UK Meteorological Office, observation period about 10 years), where these differences are found from 1.5 to 5.5% for  $u < 0.5 \text{ m s}^{-1}$ . The representative weather categories based on standard hourly UK Meteorological Office data for locality Herstmonceux over the 10-year

**Table 1**

Selection of low wind speed ( $<0.5 \text{ m s}^{-1}$ ) continuous sequences SEQ\* with duration  $\geq 3 \text{ h}$ .

NPP (year)	N(SEQ*)	P(SEQ*)	L(SEQ*) <sub>max</sub>
	number of SEQ*	percentage of SEQ*	longest SEQ* (hours)
EDU (2018)	28	1.574	12
EDU (2017)	51	2.789	10
EDU (2016)	58	3.052	10
EDU (2015)	50	2.675	14
EDU (2014)	51	4.122	11
ETE (2018)	79	4.529	15
ETE (2017)	76	4.305	20
ETE (2016)	98	5.292	11
ETE (2015)	100	5.406	14
ETE (2014)	126	8.266	18
ETE (2008–2009) <sup>a</sup>	230	8.737	35

<sup>a</sup> 17,520 hourly records.

period 1981–1990 are published in (NRPB-R302, 1999). The percentage frequency with low wind speed conditions ( $u < 1 \text{ m s}^{-1}$ ) is 22.9%, the calm ( $u < 0.5 \text{ m s}^{-1}$ ) is 5.6% (averaged over all Pasquill stability categories). Similar results are published in (Jones, 1996).

Long-term meteorological records in the territory of the Czech Republic assess the probability of low wind ( $<2.0 \text{ m s}^{-1}$ ) meteorological episodes occurrence in a wide range from a few percent up to about 14%. The duration of the situation varies from tens of minutes up to several hours. We have analysed long-term series (period 5 years) of the archived hourly meteorological data forecasted for the points of the nuclear power plant (NPP) localities provided by the Czech hydro-meteorological service.

A specific pre-processing of the archived data has been carried out for purposes of this article. The sequences denoted as SEQ\* with at least three uninterrupted consecutive data records (hours) with low wind speed  $< 0.5 \text{ m s}^{-1}$  have been collected. The results in Table 1 for locations of the NPP EDU<sup>7</sup> and NPP ETE<sup>8</sup> indicate a wide variability for different localities and time periods.

Although the probability of a long low wind speed episode is small (see beginning of this part), possible radiological impacts on the surrounding environment can be serious. Such conditions should be considered in risk assessments or safety cases, because the low wind speed conditions are likely to produce many of the worst case dispersion scenarios (Lines et al., 2001, NRPB-R302, 1999), especially for the situations where radioactive clouds would form close to the ground.

The problem of low wind speed can be theoretically treated as a continuous release, traditionally described in representations of the Gaussian dispersion models. It was generally believed that the commonly used steady-state Gaussian dispersion models, such as AERMOD (EPA, 2004) or ADMS (Carruthers et al., 2003), are not applicable to situations when the wind speed close to the ground is comparable to the standard deviation of the horizontal velocity fluctuation. The performance of the Gaussian dispersion models is poor and the concentration values during the case of the low wind speed episodes are highly over-predicted. Formerly, certain approximations were proposed for solution of the calm problem. The idea intended in the European environmental code RODOS (Real time Online DecisiOn System) assumed the equivalent plume segment slowly returning many-times alternately over the source.

An important new option addresses the former over-predicted concentration estimates. This option increases the minimum horizontal turbulence and incorporates a modified meander component. An

<sup>7</sup> Nuclear Power Plant in locality Dukovany

<sup>8</sup> Nuclear Power Plant in locality Temelín.

**Table 2**

A sequence of hourly meteorological data which could be considered as calm (blue records). Provided from the archives of the Czech Hydro-Meteorological Service for coordinates of the NPP EDU, started on Oct. 25, 2015 at 03.00 CET.

Time_stamp	Pasquill_cat.	wind_speed	wind_dir.	rain
yyyymmddhh	of atmos. stability	at 10 m height $\text{m}\cdot\text{s}^{-1}$	(°) <sup>a</sup>	mm. $\text{hour}^{-1}$
.....	.....	.....	.....	.....
2015102423	C	0.7	138	0
2015102500	D	0.8	52	0
2015102501	D	0.5	18	0
2015102502	D	0.5	26	0
2015102503	D	0.4	298	0
2015102504	F	0.3	304	0
2015102505	F	0.2	85	0
2015102506	F	0.2	170	0
2015102507	F	0.2	172	0
2015102508	C	0.3	229	0
2015102509	B	0.2	110	0
2015102510	B	0.2	339	0
2015102511	B	1.9	324	0
2015102512	C	2.1	341	0
2015102513	C	3.3	0	1.0
2015102514	D	3.3	333	1.0
.....	.....	.....	.....	.....

<sup>a</sup> Clockwise, from North.

interesting result has brought a comparison with an application of the Lagrangian dispersion model (Rakesh et al., 2019) for the case of the low wind speed conditions. The performances of the Gaussian model with improved dispersion parameters and a specific Lagrangian dispersion model are in a good mutual agreement (Anfossi et al., 2006). A profound overview of the significant references and methodology improvements is given in (Pandey and Sharan 2019).

This paper introduces a simplified scenario for the real calm situation when radioactive pollution is discharged into motionless surroundings. The generally used algorithms for a Gaussian puff model (e.g., (Adriaensen et al., 2002)) seem to be suitable for these purposes. Development of the puff model for a sequence of discrete discharges is described in that paper. In this way, the potential strong changes of the release dynamics of the harmful substances can also be simulated by sequences of different short-term instantaneous puffs. The important question related to the strict definition  $u = 0 \text{ m s}^{-1}$  for the calm situation is illustrated in the following example: The real sequence of eight hourly meteorological inputs in Table 2 (blue) shows very low wind speeds with more or less chaotic fluctuations. Moreover, the trajectory constructed from these eight points (*wind speed*, *wind direction*) is restricted to a very close region. We assume that such situations are well approximated by the calm situation ( $u \rightarrow 0 \text{ m}\cdot\text{s}^{-1}$ ) with a duration of 8 h. The wind rising in the ninth hour breaks up the calm situation.

### 3.2. Case CALM: an approximation based on a series of consecutive discrete puffs released into the stationary (motionless) ambience

Radiological consequences of a release of radionuclides during the calm conditions are treated as superposition of an equivalent chain of Gaussian puffs from the elevated source. Each puff has its own nuclide inventory and strength of released activity. The entire release is assumed to proceed under zero horizontal wind speed and each puff has a shape of a gradually-spreading discus with its centre at the source of the pollution. The radioactivity concentration in the air is described by the Gaussian-puff distribution where the vertical and horizontal dispersion coefficients are expressed by time-dependent empirical recommendations based on the field measurements under low wind speed conditions (Okamoto et al., 2001). Similarly, the calm wind dispersion parameters for the puff model in the RASCAL code (McGuire et al., 2007) are switched from distance-based to time-based entities. Each puff is modelled at all consecutive time stages, taking into account the

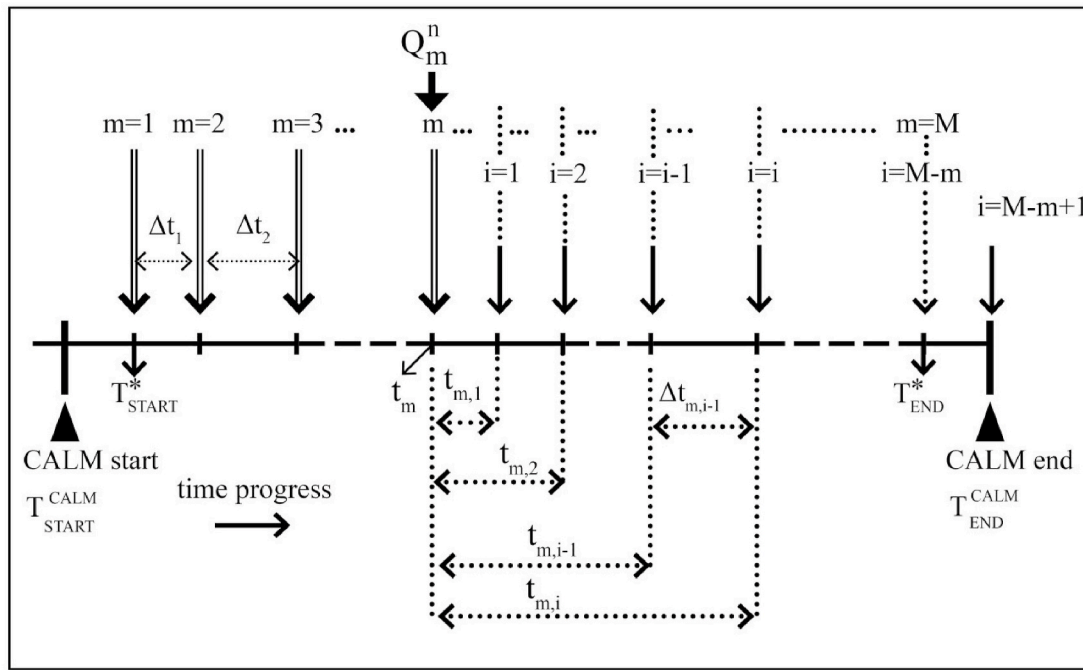


**Fig. 1.** The original detailed scheme of the time progress of the discrete radioactivity discharges into the motionless ambience during the calm meteorological episode. The discharge  $Q_m^n$  propagates during its successive relative time intervals  $i$  until the calm end.

depletion of activity due to the removal mechanisms of radioactive decay, dry activity deposition on the ground, and washout caused by the atmospheric precipitation. The dry deposition during the calm is roughly estimated when only a certain fraction corresponding to the gravitational settling is considered.

The total number  $M$  of discrete pulses  $m$  of radionuclide  $n$  are released from an elevated point source at a height  $H$  ( $x = 0; y = 0; z = H$ ) inside the mixing layer during the calm episode in the time interval  $(T_{START}^{CALM}, T_{END}^{CALM})$ . The first pulse starts at the beginning of the accident  $T_{START}^*$ . A chain of the corresponding discrete releases  $Q_m^n, m \in \{1, \dots, M\}$  are ejected step by step with the consecutive time periods  $\Delta t_m$ . This situation is demonstrated on Fig. 1, where one particular discharge  $Q_m^n$  (belonging to puff  $m$ ) propagates in its further successive relative time steps  $i$ . The originality of the scheme in Fig. 1 is implied by the fact that various parameter changes among the pulses  $m$  inside the calm region can be taken into account (release source strength, isotopic composition, atmospheric stability class, rainfall, and possibly the height of release  $H$ ). The continuous release can be simulated using a large number of discrete pulses  $m$ .

Let the  $m$ th puff be born at the starting point of the interval  $\Delta t_m$ , that is, at time  $t_m = \sum_{k=1}^{m-1} \Delta t_k$  after the beginning of accident. The pulse discharge  $Q_m^n$  (in Bq) of radionuclide  $n$  just at the starting point of the interval  $\Delta t_m$  can be different for each adjacent discharges. As stated above, it relates to the period of duration, specific group of leaking radionuclides with specific source strength, occurrence of atmospheric precipitation, etc. The source strength from the elevated source at a height  $H$  ( $x = 0; y = 0; z = H$ ) for the time period  $\Delta t_m$  is denoted by  $S_m^n(t)$  (in Bq/s). For discrete puffs, we use a symbolic notation

$$Q_m^n = \int_{(\Delta t_m)} S_m^n(t) \cdot dt \quad (3.1)$$

Where, for an instantaneous puff, the source strength can be expressed with the aid of the delta function around  $t_m$ .

We shall focus on diffusion of one particular puff  $m$  in its further stages until the moment  $T_{END}^{CALM}$ . It propagates within the consecutive time sub-intervals  $i, (i = 1, \dots, M-m+1)$  relative to  $m$ . The ‘‘age’’ of the original puff  $m$  at the end of its successive relative interval  $i$  is denoted by

$$t_{m,i} = \sum_{k=1}^{i-1} \Delta t_{m,k}. \text{ The layout is drawn on Fig. 1.}$$

Detailed mathematical formulation of the problem and derivations of the expressions are given in (Pecha et al., 2020). A brief overview of the algorithm follows.

The activity concentration  $C^n(t; x, y, z)$  [Bq/m<sup>3</sup>] of radionuclide  $n$  in the air is generally described by the Gaussian 3-D puff formula (e.g., Zannetti, 1990; Carruthers et al., 2003). We assume stable conditions and no atmospheric inversion. Let the solution consider only one reflection in the ground plane. Additional simplifications assume that the puff shape is symmetrical in the  $x$  and  $y$  directions and can be replaced by the horizontal distance  $r$  from the centre of the puff. Further specific formulation comes out directly from the terminology introduced in Fig. 1.

Propagation of radioactivity  $Q_m^n(t)$  of pulse  $m$  in time  $t$  (relatively to its ‘‘birth time’’) is modelled in discrete consecutive time intervals  $i$ . The stepwise procedure used here means that, for each interval  $i$ , the puff ‘‘stays on’’ here for the time period  $\Delta t_{m,i}$ , submitted to the specific characteristics of the atmospheric state (precipitation, stability class) that is unique for each period  $i$ . For this reason, we must formulate the scheme in a more complicated stepwise form in order to comply with the specific characteristics. It means that, instead of one course through the puff birth to its end, the propagation of the puff  $m$  should be simulated and recorded in the discrete successive time steps  $i, (i = 1, \dots, M-m+1)$ . The symbol  $C_{m,i}^n(\tilde{t}_{m,i}; r, z)$  now stands for the radioactivity concentration within the  $i$ -th interval  $\Delta t_{m,i}$ . Let  $\tau$  means the relative time inside the interval  $\Delta t_{m,i}, \tau \in (0, \Delta t_{m,i})$  and  $\tilde{t}_{m,i}$  mean the total time from birth of  $m$  until the true time of propagation within  $i$  given by  $\tilde{t}_{m,i} = t_{m,i-1} + \tau$ . The equation for the concentration shape within the interval  $\Delta t_{m,i}$  can be expressed (provided that  $\sigma_x = \sigma_y = \sigma_r, x^2 + y^2 = r^2$ ; only one reflection from ground level is accepted) in the form:

$$C_{m,i}^n(\tilde{t}_{m,i}; r, z) = \frac{Q_{m,i}^n(\tilde{t}_{m,i})}{(2\pi)^{3/2} \cdot \sigma_r^2(\tilde{t}_{m,i})} \cdot \exp\left(-\frac{r^2}{2 \cdot \sigma_r^2(\tilde{t}_{m,i})}\right) \times \quad (3.2)$$

$$\times \frac{1}{\sigma_z(\tilde{t}_{m,i})} \left\{ \exp\left(-\frac{(z-h_{ef,m})^2}{2\sigma_z^2(\tilde{t}_{m,i})}\right) + \exp\left(-\frac{(z+h_{ef,m})^2}{2\sigma_z^2(\tilde{t}_{m,i})}\right) \right\}$$

$$Q_{m,i}^n(\tilde{t}_{m,i}) = Q_m^n \cdot f_R^n(t_m \rightarrow \tilde{t}_{m,i}) \cdot f_F^n(t_m \rightarrow \tilde{t}_{m,i}) \cdot f_W^n(t_m \rightarrow \tilde{t}_{m,i}) \quad (3.3)$$

Eq. (3.3) expresses the actual form of the „source depletion“ scheme combined from the depletion factors  $f_R^n$ ,  $f_F^n$ ,  $f_W^n$  for radioactive decay, fallout on terrain, and washout by rain; it represents the radionuclide depletion from the time of birth until the true time of propagation  $\tilde{t}_{m,i}$ . A detailed comparison of the “source depletion” and an alternative “surface depletion” approach can, e.g., be found in Horst (1977).

$$f_F^n(\Delta t_{m,k}) = \frac{Q_{m,k}^n(t_{m,k})}{Q_{m,k}^n(t_{m,k-1})} = \exp \left\{ -\sqrt{\frac{2}{\pi}} \cdot v g_{grav}^n \int_{\tau=0}^{\tau=\Delta t_{m,k}} \left[ \frac{1}{\sigma_z(\tilde{t}_{m,k})} \cdot \exp\left(-\frac{h_{ef}^2}{\sigma_z^2(\tilde{t}_{m,k})}\right) \right] d\tau \right\} \quad (3.7)$$

### 3.2.1. Depletion of stationary puff due to radioactive decay

The radioactive decay is accomplished throughout the entire puff volume. The corresponding depletion in  $\langle t_0; t \rangle$  generally proceeds proportionally to  $\exp[-\lambda \cdot (t-t_0)]$ . Specifically, the depletion of the original puff  $m$  until its relative interval  $i$  is driven according to

$$f_R^n(t_{m,i}) = \prod_{k=1}^{k=i} \exp(-\lambda^n \cdot \Delta t_{m,k}) = \exp(-\lambda^n \cdot t_{m,i}) \quad (3.4)$$

where  $\lambda^n$  [s<sup>-1</sup>] denotes the constant of the radioactive decay.

### 3.2.2. Depletion of stationary puff due to dry deposition (FALLOUT<sup>9</sup>)

Depletion of the puff activity concentration due to the process of dry deposition results from both the gravitational settling and the interaction within the surface layer. The smaller aerosol particles (0.1–1 μm) survive for a long time in the plume, and their depletion from the plume is mainly caused by their interaction with the surface structures (depending on roughness and friction velocity). In general, the values of the gravitational settling speed vary, depending on the atmospheric stability, wind speed and surface conditions. For calm conditions, we shall restrict our consideration to a simplified recommendation, related only to the process of gravitational settling for the aerosol particles. The properties of the particles play an important role in the radiological hazard. This process is significant for particles with higher diameter values, which do not remain airborne for a long time. A brief summary of the gravitational settling is, e.g., described in (Hanna et al., 1982; Pöllänen et al., 1995; Baklanov and Sorensen, 2001). The sedimentation velocity as a function of particle aerodynamic diameter, particle shape, particle composition, surface characteristics, charge or possible coagulation processes is studied in-depth in (Tsuda et al., 2013). The roughly estimated value  $v g_{grav}^n = 0.008 \text{ m}\cdot\text{s}^{-1}$  is used there. It could be accepted as an upper limit for the aerosol particles with radii about 5–10 μm.

Let us again take the relative time variable  $\tau$  from the interval  $\Delta t_{m,k}$ ,  $\tau \in \langle 0, \Delta t_{m,k} \rangle$ ;  $k = 1, \dots, i$ . We search for the total activity in the puff  $Q_{m,k}^n(\tilde{t}_{m,k})$ ;  $\tilde{t}_{m,k} = t_{m,k-1} + \tau$  within the interval  $\Delta t_{m,k}$  corresponding to  $Q_{m,k}^n(\tilde{t}_{m,k}) \in \langle Q_{m,k}^n(t_{m,k-1}), Q_{m,k}^n(t_{m,k}) \rangle$ . The near-ground activity concentration  $C_{m,k}^n(\tilde{t}_{m,k}; r, z = 0)$  in the interval  $\tau \in \langle 0, \Delta t_{m,k} \rangle$  is gradually depleted according to Eqs. (3.2) and (3.3). The total dry deposition flux on the ground  $\dot{Q}_{m,k}^n(t; z = 0)$  [Bq.s<sup>-1</sup>] from the whole puff ( $m,k$ ), just at its

position at time  $\tilde{t}_{m,k}$ , is given by

$$\dot{Q}_{m,k}^n(\tilde{t}_{m,k}; z=0) = \int_0^\infty v g_{grav}^n \cdot C_{m,k}^n(\tilde{t}_{m,k}; r, z=0) \cdot 2\pi \cdot r \cdot dr \quad (3.5)$$

The source strength reduction inside the interval  $\Delta t_{m,k}$  due to the deposits on the ground is expressed as

$$dQ_{m,k}^n(t)/dt = - \dot{Q}_{m,k}^n(t; z=0) \quad (3.6)$$

The near-ground activity concentration  $C_{m,k}^n(\tilde{t}_{m,k}; r, z = 0)$  from Eq. (3.2) is substituted here and, after integration, the resulting partial deposition factor of the pulse  $m$  of radionuclide  $n$  on the ground during the period  $\Delta t_{m,k}$  due to the fallout is determined as follows:

The final form of the total dry deposit (FALLOUT) depletion factor  $f_F^n(t_m \rightarrow t_{m,i})$  for the puff  $m$  from its birth until the  $i$ -th time interval is given as a product of all partial depletion factors for the respective  $k$  until  $i$ :

$$f_F^n(t_m \rightarrow t_{m,i}) = Q_{m,i}^n / Q_m^n = \prod_{k=1}^{k=i} f_F^n(\Delta t_{m,k}) \quad (3.8)$$

### iii. Wet deposition (WASHOUT<sup>10</sup>) from stationary puff

The radioactivity concentration of radionuclide  $n$  in the puff  $m$  (originally born at the moment  $t_m$ ) during its next stages  $i$  is expressed by Eq. (3.2). We assume the rain at a constant precipitation rate  $v_{m,i}$  [mm·h<sup>-1</sup>] during the entire interval  $\Delta t_{m,i}$ . The deposition activity rate of nuclide  $n$  being washed out from the cloud is expressed using washing coefficient  $\Lambda_{m,i}^n = a \cdot v_{m,i}^b$  [s<sup>-1</sup>]. Constants  $a$  and  $b$  depend on the physical-chemical form of the radionuclide  $n$  (they are different for aerosol, elemental, organic form, and zero for noble gases – revised knowledge in (Sportisse, 2007)).

Let us assume that the relative time variable  $\tau$  lies in the interval  $\Delta t_{m,k}$ ,  $\tau \in \langle 0, \Delta t_{m,k} \rangle$  and it is raining inside the interval. We search for the distribution of the total activity in the puff  $Q_{m,k}^n(\tilde{t}_{m,k})$ ,  $\tilde{t}_{m,k} = t_{m,k-1} + \tau$ , within the interval  $\Delta t_{m,k}$  corresponding to  $Q_{m,k}^n(\tilde{t}_{m,k}) \in \langle Q_{m,k-1}^n, Q_{m,k}^n \rangle$ . The activity concentration  $C_{m,k}^n(\tilde{t}_{m,k}; r, z)$  in the interval  $\tau \in \langle 0, \Delta t_{m,k} \rangle$  is gradually depleted by washout. The total wet deposition flux  $\dot{W}_{m,k}^n$  [Bq.s<sup>-1</sup>] from the puff ( $m,k$ ) (puff  $m$  in its successive time interval  $k$ ) at the time  $\tilde{t}_{m,k}$  is given by

$$\dot{W}_{m,k}^n(\tilde{t}_{m,k}) = \int_0^\infty \left[ \Lambda_{m,k}^n \cdot \int_0^\infty C_{m,k}^n(\tilde{t}_{m,k}; r, z) \cdot dz \right] \cdot 2\pi \cdot r \cdot dr \quad (3.9)$$

The source strength reduction in the interval  $\langle 0, \Delta t_{m,k} \rangle$  due to the wet deposition on the ground is expressed as

$$dQ_{m,k}^n/dt = - \dot{W}_{m,k}^n \quad (3.10)$$

After substitution and integration, the resulting partial factor due to

<sup>9</sup> Fall of radioactivity on the ground.

<sup>10</sup> Washing of radioactivity from cloud due to atmospheric precipitation.

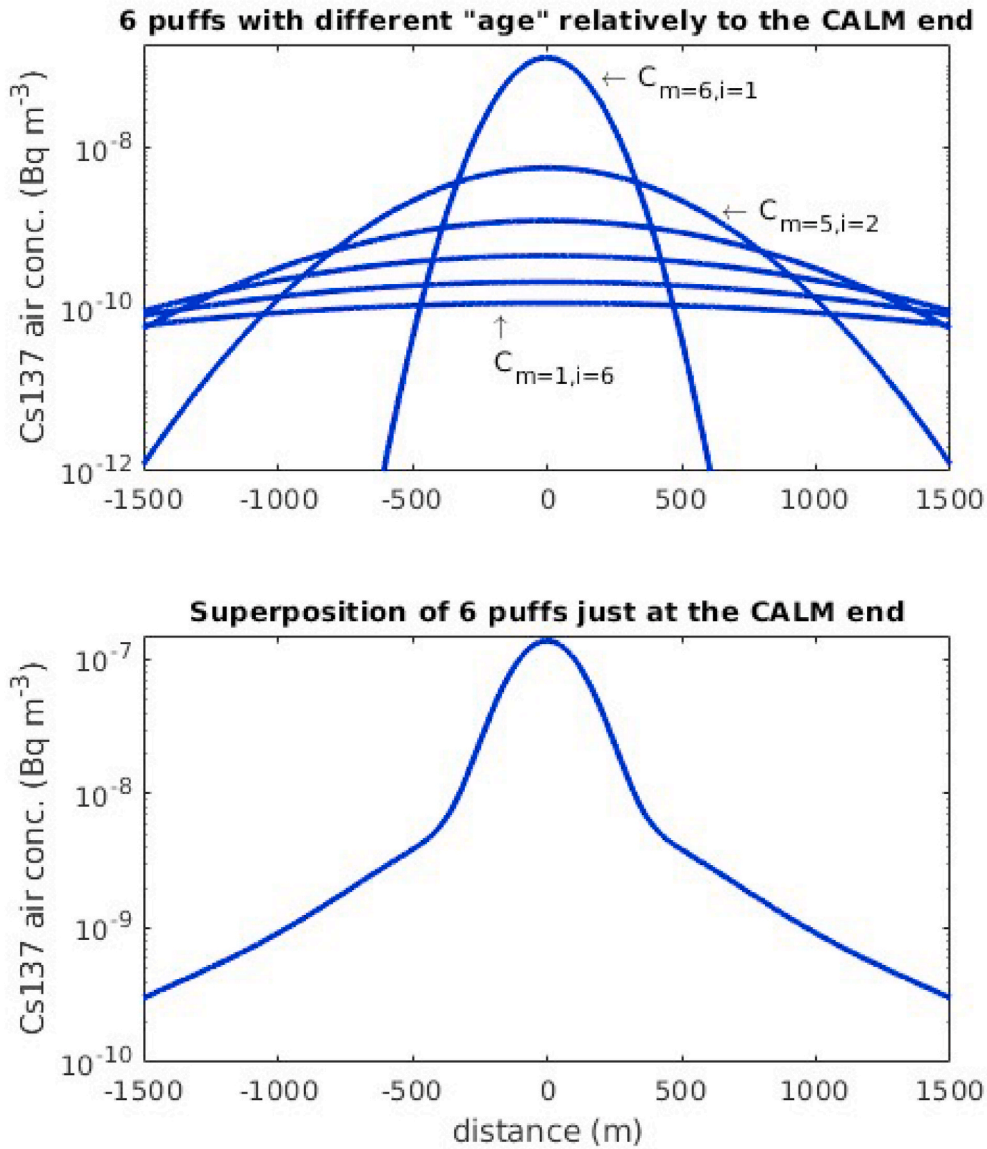


**Fig. 2.** During calm period 2 h, 6 discrete pulses  $m$  are released, each in period 20 min. Particular puff  $m$  reaches  $T_{END}^{CALM}$  moment with concentration  $C_{m,i}$ ,  $i = 6-m+1$  ( $C_{m=6,i=1}$  for the youngest puff  $m = 6$ ,  $C_{m=1,i=6}$  for the oldest puff  $m = 1$ ). Evidently non-Gaussian distribution composed from the individual discrete Gaussian puffs (top) is given below. The results of the calm situation are related just to the moment  $T_{END}^{CALM}$ .

---


$$f_W^n(\Delta t_{m,k}) = \frac{Q_{m,k}^n(t_{m,k})}{Q_{m,k}^n(t_{m,k-1})} = \exp \left\{ -\sqrt{\frac{2}{\pi}} \cdot A_{m,k}^n \cdot \int_{\tau=0}^{\tau=\Delta t_{m,k}} \left[ \int_0^\infty \Psi \left( z, \sigma_z(\tilde{t}_{m,k}), h_{ef,m} \right) \cdot dz \right] d\tau \right\} \quad (3.11)$$


---

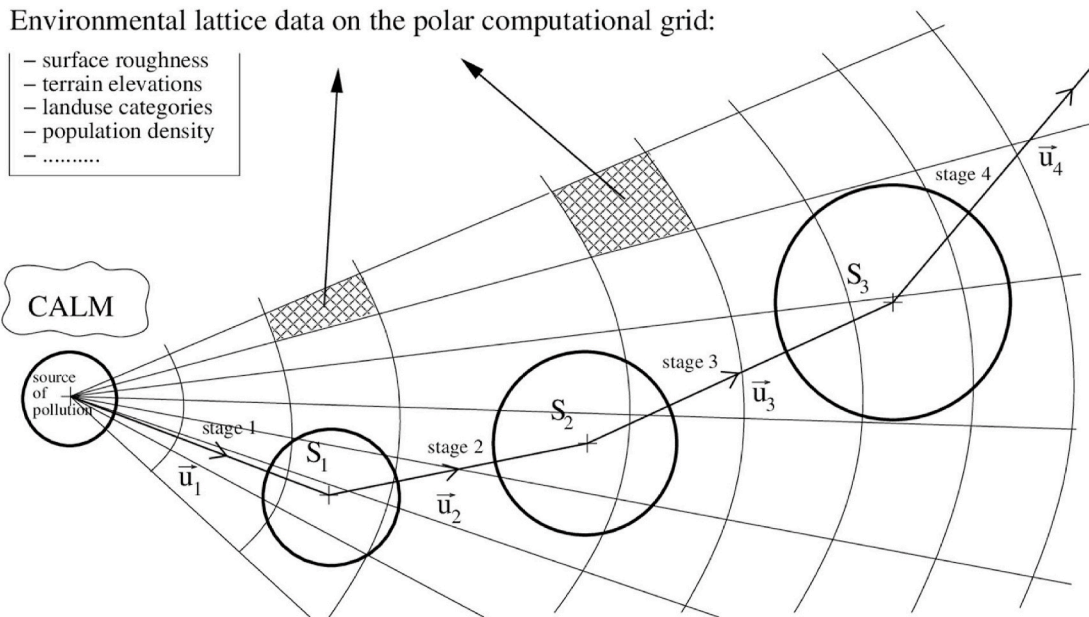


Fig. 3. Drift of the CALM results in the next hours of the convective flow. Propagation directed by hourly forecast of the meteorological conditions. Environmental grided data enter the calculations.

washout in period  $\Delta t_{m,k}$  is determined as

$$\text{where } \Psi(z, \sigma_z(\tilde{t}_{m,k}), h_{ef,m}) = \frac{1}{\sigma_z(\tilde{t}_{m,k})} \left\{ \exp\left(-\frac{(z-h_{ef,m})^2}{2\cdot\sigma_z^2(\tilde{t}_{m,k})}\right) + \exp\left(-\frac{(z+h_{ef,m})^2}{2\cdot\sigma_z^2(\tilde{t}_{m,k})}\right) \right\}$$

The final form of the washout depletion factor  $f_W^n(t_m \rightarrow t_{m,i})$  for the puff  $m$  from its birth  $k = 1$  until the  $k = i$  is given as a product of all partial wet depletion factors for respective  $k$  until  $i$ :

$$f_W^n(t_m \rightarrow t_{m,i}) = Q_{m,i}^n / Q_m^n = \prod_{k=1}^{k=i} f_W^n(\Delta t_{m,k}) \quad (3.12)$$

*Comment:* For rain episode, the algorithm should be somewhat adjusted. Let us assume it is raining at the start of the pulse  $m^*$ . The previous pulses  $m \leq m^*$  are already “on the road” in their respective relative stages  $i$  (for better understanding we use label  $i(m)$ ). We should consider the relative stage  $i(m)$  of the pulse  $m$  as wet (washed out), provided that:

$$i(m) = m^* - m + 1; m \leq m^*$$

#### 4. Evaluation of radiological quantities just at the moment $T_{END}^{CALM}$ of the calm episode termination

The radioactivity accumulated in the stationary ambient atmosphere is given by superposition of results of all partial pulses  $m$  in their final stages just when reaching the end of the calm period. The total overall radioactivity concentration in the stationary package of air at the moment of the calm termination can, in agreement with the sketch shown in Fig. 1, be schematically expressed as

$$C_n(T_{END}^{CALM}; r, z)^{TOTAL} = \sum_{m=1}^{m=M} C_{m,i=M-m+1}^n(r, z) \quad (4.1)$$

where  $C_{m,i=M-m+1}^n(r, z)$  is constructed according to the scheme in Fig. 1.

The total package of radioactivity just at the calm end  $T_{END}^{CALM}$  consists of superposition of multiple Gaussian puffs  $m$ , each with the concentration value  $C_{m,i=M-m+1}^n$ . It belongs to the original partial discharge of radioactivity  $Q_m^n$ , which dissipates into the motionless ambient until the calm termination. As stated above, the first stage of the scenario after the calm terminates is immediately succeeded by the second stage of the convective movement in the atmosphere. The wind is assumed to start blowing, which immediately drifts and scatters the original stationary heap of radioactivity over the terrain. The results of the calm situation just at the moment  $T_{END}^{CALM}$  are shown in Fig. 2. It represents the initial conditions for the description of the subsequent convective transport. One of the following two alternative procedures could provide a reasonable solution:

**ProcPP**<sup>11</sup>: The movement within each individual Gaussian puff  $m$  with activity concentration  $C_{m,i=M-m+1}^n$  from (4.1) is treated separately in all of its consecutive convective stages. The resulting radiological quantities are given by the superposition for all puffs  $m$ .

**Superpuff**<sup>12</sup>: The algorithm developed here for the convective transport is based on Gaussian puffs. But a superposition of all partial puffs  $M$  is evidently non-Gaussian (bottom in Fig. 2). An attempt has been made to estimate the statistical properties of  $C^n(T_{END}^{CALM}; r, z)^{TOTAL}$  in advance and examine a possibility to substitute the Gaussian mixture drifted by wind with a sole representative equivalent Gaussian *Superpuff* distribution (Kárný and Guy, 2012). The benefit in reduction of computational load should be evident, mainly for a large value of  $M$  (simulation of the continuous release) and introduction of advanced dispersion code. Schematic notation of the *Superpuff* Gaussian approximation of the probability density distribution is denoted by

$$N^{super}(\mu^x, \Sigma^x) \quad (4.2)$$

$p$ -dimensional random vector  $x$  has the mean values  $\mu^x$ , and  $\Sigma^x$  is the covariance matrix of its components (for a specific formulation for the

<sup>11</sup> Acronym for the time consuming but accurate solution of multi-pulse approach.

<sup>12</sup> Acronym for the new statistical approximate solution of multi-phase approach.

case  $p = 2$  - see expression (6.1) below). The first results of comparing both procedures are shown in Section 6, Fig. 6 and Fig. 7.

### 5. Immediate drift of stationary heap of radioactivity accumulated during previous calm episode according to changes of the meteorological conditions

The calm region is assumed to be suddenly submitted by wind. An elementary basic formulation for small-scale advection of puffs under stable and neutral conditions is adopted. The puffs are assumed to be symmetrical in  $x$  and  $y$  directions and can be replaced by the horizontal distance  $r$ . The centre of the puff is linearly moving in the direction of the wind within each consecutive convective stage  $p$ . The relative diffusion with regard to the puff centre is in progress. Hourly changes in the meteorological situation are available and a segmented Gaussian puff model is used. Within each hour, the propagation is straightforward and changes are coming up all at once for a given hour. This paper focuses on the near-field analysis in a smaller domain and below the mixing layer. We do not yet consider more sophisticated but computationally expensive modelling that would account for puff meandering or puff furcation.

We shall follow the procedure **ProcPP** from Section 4. The individual discharge  $Q_m^n$  was gradually spreading inside the original calm region in such a way that the corresponding partial radioactivity concentration in the air at the moment  $T_{END}^{CALM}$  is denoted by  $C_{m,i=M-m+1}^n$ , alias  $C_m^n(T_{END}^{CALM}; r, z)$ . The original position of the previous calm region centre was  $(x = 0; y = 0; z = H)$ . The convective movement in the direction of  $\vec{u}_1$  starts from there at  $T_{END}^{CALM}$ . The movement of the puff at each stage  $p$  is assumed to be composed from the absolute overall straight-line translations with velocity values  $\vec{u}_p$  and relative dispersions around the puff centre with the dispersion parameters dependent on the translation shifts. Available hourly meteorological data enables us to account, step by step, for relevant scenario parameter changes (see the sketch in Fig. 3).

The Gaussian puff model describing the further convective movement of the radioactivity from the calm region is adapted. The initial distribution of concentration entering the first convective stage  $p = 1$  is determined as  $C_m^n(r, z; T_{END}^{CALM})$ . Depletion of the original discharge  $Q_m^n$  from its birth at  $t_m$  until  $T_{END}^{CALM}$  is, in agreement with (3.3), expressed as

$$Q_m^n(T_{END}^{CALM}) = Q_m^n(t_m) \cdot f_F^n(t_m \rightarrow T_{END}^{CALM}) \cdot f_R^n(t_m \rightarrow T_{END}^{CALM}) \cdot f_W^n(t_m \rightarrow T_{END}^{CALM}) \quad (5.1)$$

This expression belongs to the low wind speed conditions formulated in the time-representation. For the convective transport, the equivalent expression should be formulated on the distances passed along the puff trajectory when the types of land-use and orography are incorporated. The parcel of radioactivity is successively drifted at hourly intervals (stages)  $p$  ( $p = 1, \dots$ ) with the velocity values  $\vec{u}_p$  and with other parameters of this scenario pertaining to the hourly changes in the stage  $p$ . The length of the puff centre shift within a particular stage  $p$  is denoted by  $l_p$ , the total length of the puff centre from the beginning of the first stage  $p = 1$  until the end of stage  $p$  is denoted by  $L_p$ . The radioactivity dispersion and depletion take place within the convective stages  $p$ . For the end of the  $p$ th stage of the convective transport, the initial discharge  $Q_m^n(T_{END}^{CALM})$  is further reduced by the depletion factor  $F_{conv}^n$ , which coincides with the puff progress:

$$F_{conv}^n(L_p) = f_R^n(L_p) \cdot f_F^n(L_p) \cdot f_W^n(L_p) \quad (5.2)$$

This accounts for all possible mechanisms of activity removal pertaining to the convective transport of the puff.  $L_p = (|\vec{u}_1| + |\vec{u}_2| + \dots + |\vec{u}_p|) \times 3600 = \sum_{k=1}^{k=p} l_k$  (in [m]) is a sum of the lengths of the straight-line parts of the puff's central trajectory until the end of stage  $p$  relative to the beginning of  $p = 1$ . A detailed review of relevant parameterizations for the modelling of the depletion mechanisms is given in (Sportisse, 2007). Based on the field

measurements, the parameterized models for dry deposition velocities and wet scavenging are compiled. Dispersion coefficients  $\sigma_r$  and  $\sigma_z$  should be calculated differentially, according to scheme

$$\sigma(L_p) = \sigma(T_{END}^{CALM}) + \Delta\sigma(L_p) \quad (5.3)$$

As stated above, the vertical and horizontal dispersion coefficients  $\sigma(T_{END}^{CALM})$  are expressed by time-dependent empirical recommendations based on the field measurements under low wind speed conditions. The downwind concentrations of airborne pollutants during the convective transport are determined on the basis of the coefficients of lateral and vertical dispersions. The key variable is the surface roughness during the puff-surface interaction. Semi-empirical formulae for dispersion  $\Delta\sigma(L_p)$  either for smooth terrain or, alternatively, for rough terrain of the Central European type, can be chosen for the convective flow.

The final expression for the activity concentration in the air inside the  $p$ th stage of convective transport with relative coordinate  $l \in [0; l_p]$  has a symbolic form analogous to (3.2):

$$C_{m,p}^n(l; r, z) = \frac{Q_{m,p}^n(l)}{(2\pi)^{3/2} \cdot \sigma_r^2(L_{p-1} + l)} \times \exp\left(-\frac{r^2}{2 \cdot \sigma_r^2(L_{p-1} + l)}\right) \times \quad (5.4)$$

$$\times \frac{1}{\sigma_z(L_{p-1} + l)} \left\{ \exp\left(-\frac{(z - h_{ef,m})^2}{2 \cdot \sigma_z^2(L_{p-1} + l)}\right) + \exp\left(-\frac{(z + h_{ef,m})^2}{2 \cdot \sigma_z^2(L_{p-1} + l)}\right) \right\}$$

The notation  $Q_{m,p}^n(l) = Q_m^n(T_{END}^{CALM}) \cdot F_{conv}^n(L_{p-1} + l)$  is defined for the progress of radioactivity amount within stage  $l$ , the coordinates  $(r, z)$  are assumed relative to the centre of the puff,  $\sigma(L_{p-1} + l)$  are given by (5.3). The value of  $F_{conv}^n(L_{p-1} + l)$  is the total plume radioactivity depletion inside path  $l_p$  given by (5.2).

#### 5.1. Depletion of drifted puff due to radioactive decay

The radioactive decay occurs within the entire puff volume and the corresponding depletion along the path of the particular stage  $p$  is defined as  $\exp\left(-\lambda^n \frac{l_p}{|\vec{u}_p|}\right)$ . In total, the depletion of the puff in its path from  $p = 1$  until the end of stage  $p$  can be expressed as

$$f_R^n(L_p) = \prod_{k=1}^{k=p} \exp\left(-\lambda^n \frac{l_k}{|\vec{u}_k|}\right) \quad (5.5)$$

where  $\lambda^n$  ( $s^{-1}$ ) denotes the constant of the radioactive decay,  $l_k$  is a straight line of the puff in stage  $k$ .

#### 5.2. Depletion of radioactivity in the course of convective transport due to dry deposition (FALLOUT)

Dry deposition generally means the removal of pollutants by sedimentation under gravity, diffusion processes or by turbulent transfer resulting in impacts and interception. Formulation of the radioactivity propagation over the ground is expressed in notation of the source depletion model. Roughly speaking, the model assumes that the depletion occurs over the entire depth (vertical column) rather than on the surface. The puff's vertical profile is therefore invariant with respect to distance (Hanna, 1982). However, the concentrations of activity along the axis can be somewhat over-estimated.

Let us assume the transport in the  $p$ -th stage according to Fig. 3 with the aim to determine the term  $f_F^n(L_p)$  in Eq. (5.2). The amount of radioactivity in the puff just entering stage  $p$  is labelled as  $Q_{m,L_{p-1}}^n$  and the corresponding concentration  $C_{m,p}^n(l = 0, r, z)$  is expressed in accordance with Eq. (5.4). For  $p = 1$ , the amount  $Q_{m,p=1}^n$  means radioactivity at  $T_{END}^{CALM}$  and the term  $C_{m,p=1}^n(r, z)$  means the particular component

**Table 3**

Hourly changes of meteorology conditions during the convective transport which immediately supersede the calm.

Hour	wind speed at 10 m height, m·s <sup>-1</sup>	wind direction (°) <sup>a</sup>	Pasquill categ. <sup>b</sup>	precipitation mm·hour <sup>-1</sup>
1	3.0	279	D	0.0
2	4.0	315	D	0.0
3	3.0	346	D	1.0
4	....	....	....	....

<sup>a</sup> Clockwise, from North.

<sup>b</sup> Atmospheric stability class according to Pasquill categorization.

$C_{m,i=M-m+1}^n(r, z)$  from Eq. (4.1) (identically,  $C_m^n(T_{END}^{CALM}; r, z)$ ). Specifically, let us analyse the fallout during the transport at stage  $p$  within the interval  $l \in < 0; l_p >$  when the centre of the puff is moving linearly with velocity  $\vec{u}_p$  along the abscisa  $S_{p-1}S_p$ . For the puff in relative position  $l$ , the dry deposition flux over the ground  $\dot{Q}_{m,p}^n(l; z=0)$  [Bq·s<sup>-1</sup>] from the entire puff is given by

$$\dot{Q}_{m,p}^n(l; z=0) = v g_p^n(l) \cdot \int_0^\infty C_{m,p}^n(l; r, z=0) \cdot 2\pi \cdot r \cdot dr \quad (5.6)$$

After the puff shift  $dl = u_p \cdot dt$ , the source strength reduction inside the interval  $l$  is expressed as

$$\frac{dQ_{m,p}^n(l)}{dl} = \frac{dQ_{m,p}^n(t)}{u_p \cdot dt} = - \dot{Q}_{m,p}^n(l; z=0) \quad (5.7)$$

Substituting  $C_{m,p}^n(l; r, z=0)$  from (5.4) into (5.6), and, after integration, the resulting partial deposition depletion factor of the pulse  $m$  of radionuclide  $n$  on the ground within the shift on the whole length  $l_p$  is expressed as

$$\frac{Q_{m,p}^n(L_p)}{Q_{m,p}^n(L_{p-1})} = \exp \left\{ - u_p \cdot \sqrt{\frac{2}{\pi}} \cdot \int_0^{l_p} v g_p^n(l) \cdot \frac{1}{\sigma_z(L_{p-1} + l)} \cdot \exp \left( - \frac{(h_{ef,m})^2}{2 \cdot \sigma_z^2(L_{p-1} + l)} \right) \cdot dl \right\} \quad (5.8)$$

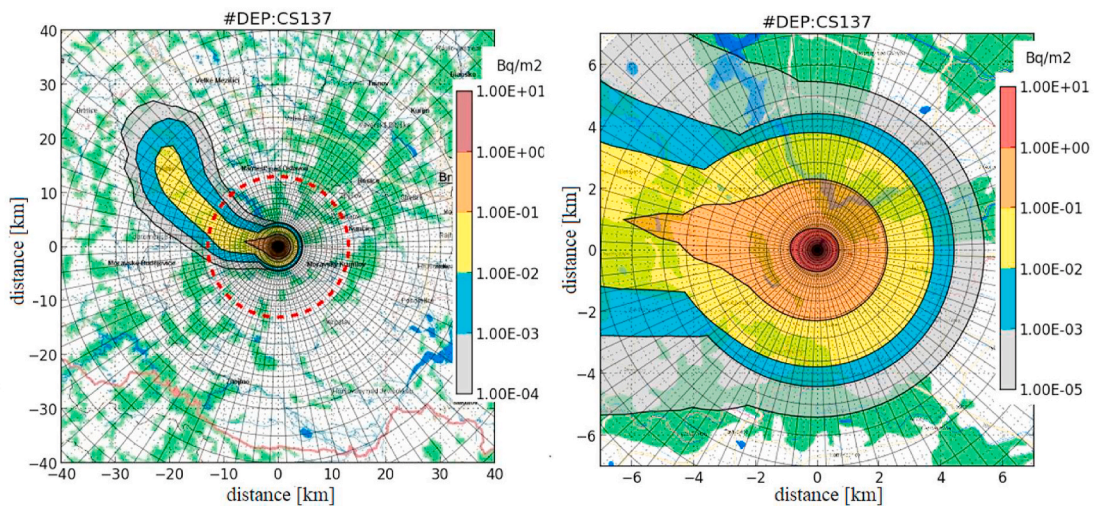


**Fig. 4.** Deposition of radionuclide <sup>137</sup>Cs on terrain (sum of 2 h calm situation plus 3 h of the instant convective movement). No atmospheric precipitation. Left: Near vicinity up to 40 km from the source of pollution. Right: More detailed image in the original calm region inside the emergency planning zone.

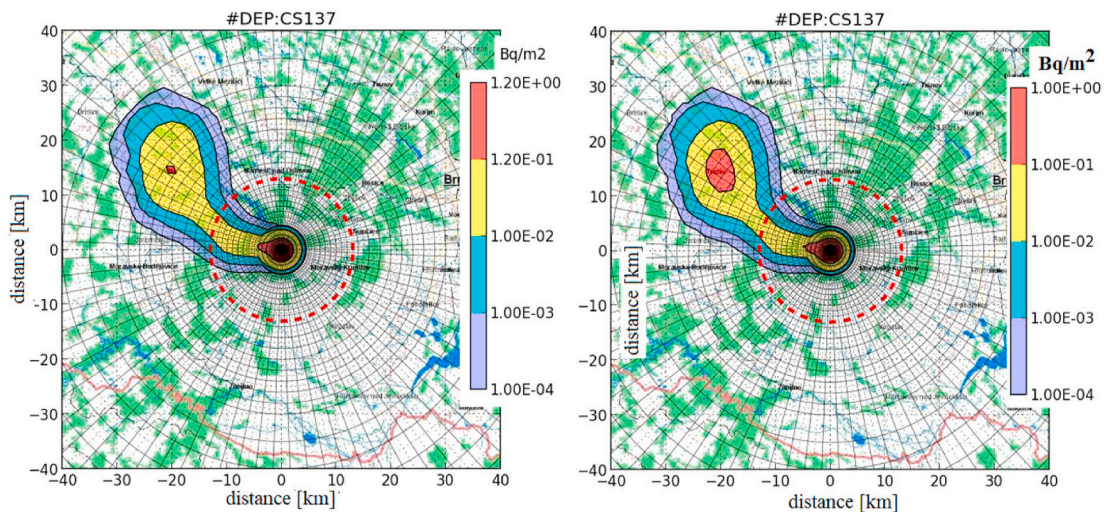


**Fig. 5.** Trajectories with “Hot spots” of deposited radionuclide <sup>137</sup>Cs on terrain. Sum of 2 h of the calm situation plus 3 h of the convective movement in the case of atmospheric precipitation in the third hour of the convective transport. Left: Rain with intensity 0.5 mm h<sup>-1</sup>. Right: Rain with intensity 1.0 mm h<sup>-1</sup>.

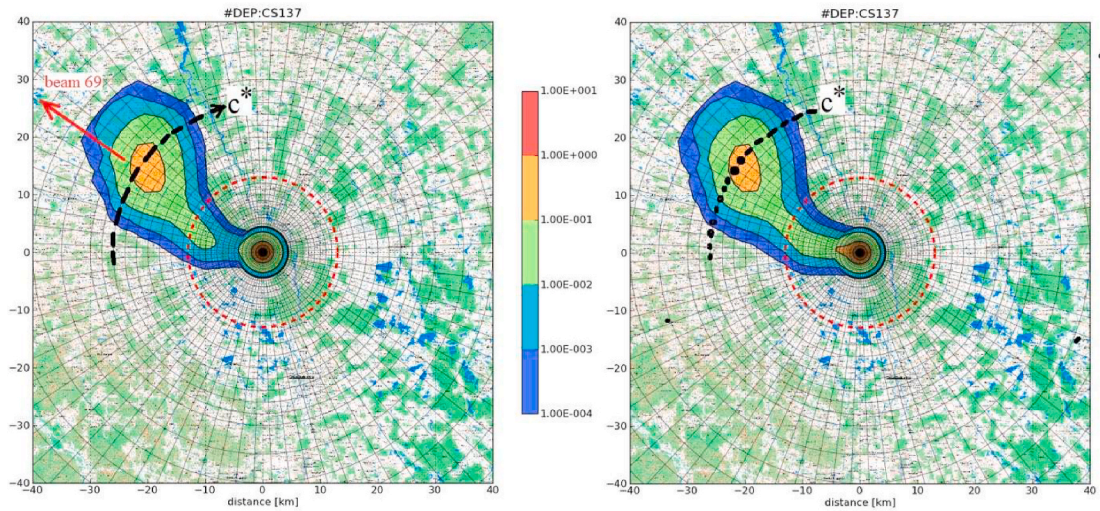


Fig. 6. Validity tests of the proposed “Superpuff” concept - Left: “Superpuff”, Right: ProcPP. Trajectory of radionuclide  $^{137}\text{Cs}$  deposition on terrain. Sum of 2 h of the calm situation plus 3 h of the convective movement. Atmospheric precipitation in the third hour of the convective transport ( $1 \text{ mm}\cdot\text{h}^{-1}$ ).

The partial fallout depletion factor for the whole stage  $p$  is designated as  $f_F^n(l_p) = Q_{m,p}^n(L_p) / Q_{m,p}^n(L_{p-1})$ . Finally, the total fallout depletion in all convective stages  $k = 1, \dots, p$  (on the path  $<0; L_p >$ ) is found as a product of all partial fallout depletion factors for each separate stage  $k$  according to:

$$f_F^n(L_p) = \prod_{k=1}^{k=p} f_F^n(l_k) \quad (5.9)$$

The integrals above are solved numerically. Strong dependency of  $v_{m,p}^n(l)$  on the spatial land-use categories of the input environmental gridded data is taken into account (indicated in Fig. 3). The identification between relative coordinate  $l$  and respective absolute land-use gridded coverage on the real terrain is established and put into operation.

### 5.3. Depletion of radioactivity in the course of the convective transport due to washout by atmospheric precipitation

Similar to Section 3.2.3, we assume rain of a constant precipitation rate  $v_{m,p}$  (mm/h) during the entire convective stage  $p$ . The deposition activity rate of nuclide  $n$  being washed out from the cloud is expressed with the aid of washing (scavenging) coefficient  $A_{m,p}^n = a \cdot (v_{m,p})^b [\text{s}^{-1}]$ . The precipitation rate  $v_{m,p}$  is averaged over the entire partial convective stage  $p$ . The wet deposition flux  $\dot{W}_{m,p}^n$  [ $\text{Bq}\cdot\text{s}^{-1}$ ] from the entire puff with its centre at relative position  $l$  of the stage  $p$  is given by

$$\dot{W}_{m,p}^n(l) = A_{m,p}^n \cdot \int_0^\infty \left[ \int_0^\infty C_{m,p}^n(l; r, z) \cdot dz \right] \cdot 2\pi \cdot r \cdot dr \quad (5.10)$$

Depletion of the radioactivity during differential shift  $dl = u_p \cdot dt$  of the puff with its centre at a relative position of  $l$  is expressed as

$$dQ_{m,p}^n(l) / dl = 1 / u_p \cdot dQ_{m,p}^n(l) / dt = -\dot{W}_{m,p}^n(l) \quad (5.11)$$

After substitution for  $C_{m,p}^n(l; r, z)$  from (5.4) into (5.10) and integration on  $l \in <0; l_p >$ , the radioactivity wet deposition flux over the ground from the entire puff is calculated. We obtain an expression for the partial source depletion of the radioactivity in the air on the rainy stage  $p$  in the form  $f_W^n(l_p) = Q_{m,p}^n(L_p) / Q_{m,p}^n(L_{p-1})$ . The total depletion is determined from the product

$$f_W^n(L_p) = Q_{m,p}^n(L_p) / Q_m^n(I_{END}^{CALM}) = \prod_{k=1}^{k=p} f_W^n(l_k) \quad (5.12)$$

## 6. Examples of background radiological field trajectories for the overall case CALM

A hypothetical release of radionuclide  $^{137}\text{Cs}$  is divided into two stages. In the first 2 h ( $\text{TCALM} = 2$ ), a calm meteorological situation is assumed. Following Fig. 1, we have adjusted  $M = 6$ . The same discharge of  $Q_m = 1.0 \text{ E}+07 \text{ Bq}$  is released into the motionless ambient every 20 min for each pulse  $m \in \{1, \dots, M\}$ . Just after 2 h of the calm, the wind starts blowing and the convective transport of the radioactivity clew immediately arises. Meteorological data are assumed to be extracted from the forecast series for a given point of the radioactive release. The hourly changes of the wind direction and velocity together with the Pasquill category of atmospheric stability were selected here for demonstration purposes (see Table 3). The data directly follows the calm condition (duration 2 h).

In the following figures, some examples are given of what the background trajectories for the overall Case CALM look like. The results of tests are displayed on the map background of the Czech nuclear power plant EDU. The total trajectory of the depositions of radionuclide  $^{137}\text{Cs}$  on the ground is indicated for a meteorological situation without rain (Fig. 4). An occurrence of atmospheric precipitation in the third hour of the convective transport is shown in Fig. 5.

Depletion of radioactive aerosols due to the processes of rainout and washout are lumped together through so-called scavenging coefficient mentioned above in Sections 3.2.3 and 5.3. A “fattening” of the washed-out radioactivity on the terrain caused by precipitation in the third hour of the convective transport is shown in Fig. 5. Its left part detects the occurrence of a small red patch of the higher level of deposited radioactivity (rain intensity  $0.5 \text{ mm}\cdot\text{h}^{-1}$ ). The right side predicates considerable impact of more intensive atmospheric precipitation (rain intensity  $1.0 \text{ mm}\cdot\text{h}^{-1}$ ) when the “hot spot” radioactivity deposition values can increase more than one order of magnitude, even in the distances of tens of kilometres from the source of pollution.

Validity tests of the proposed “Superpuff” concept from Section 4 are presented in Figs. 6 and 7. A direct but clumsy and time consuming solution ProcPP is illustrated in Fig. 6, right. The alternative “Superpuff” approximation results in trajectory in Fig. 6, left. It belongs to the statistical evaluation of the Gaussian “Superpuff” approximation given by expression (4.2) (more in (Kárný and Guy, 2012):

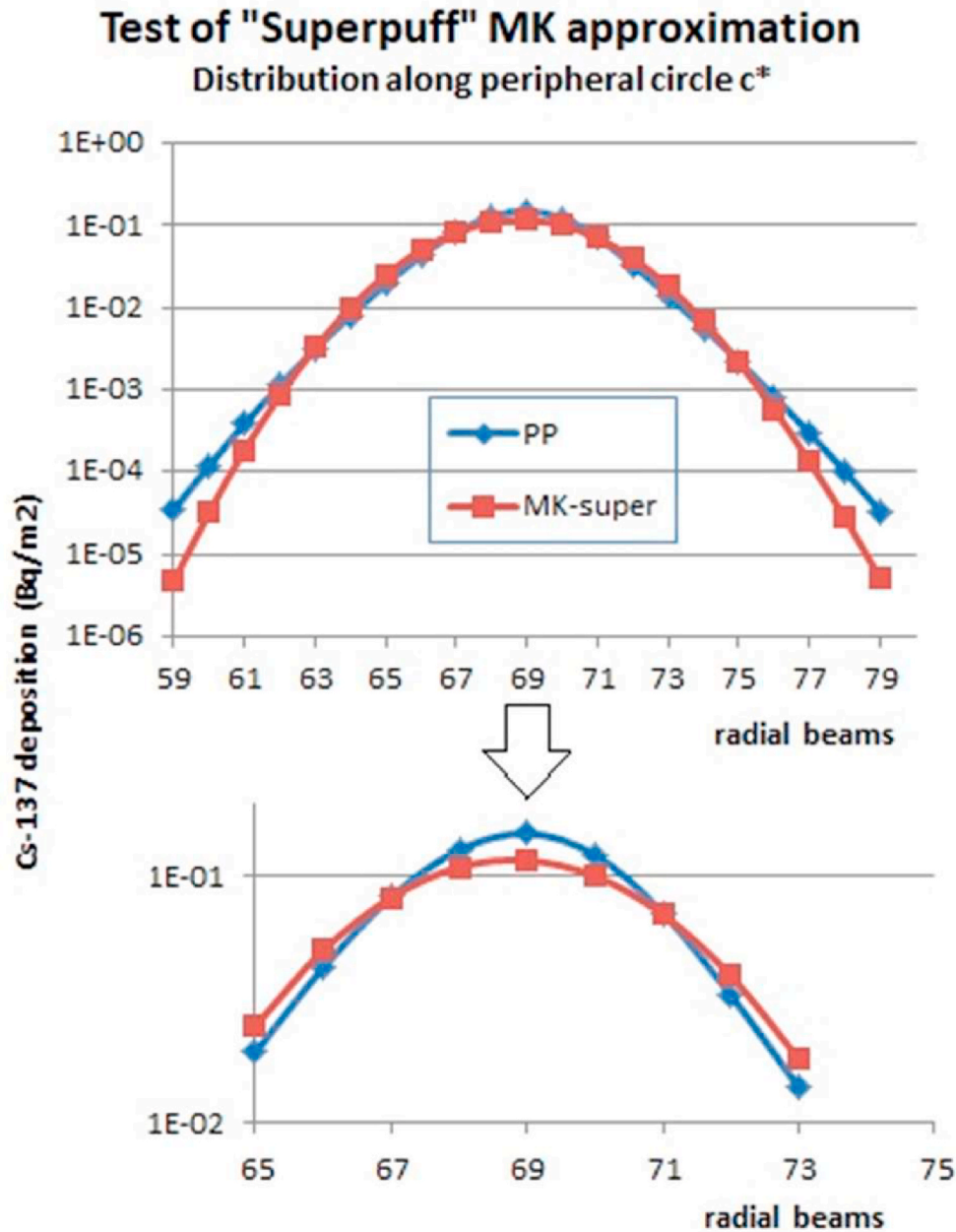


Fig. 7. Validity tests. Values of radionuclide <sup>137</sup>Cs deposition on terrain - peripheral distribution around the circle c\* (25 km from the source). Effective calculation speeding approximation based on statistical Gaussian approach “Superpuff” MK (red). Comparison with time-consuming but accurate solution ProcPP (blue). Zoom of the central part is depicted below. (For interpretation of the references to colour in this figure legend, the reader is referred to the Web version of this article.)

$$\mu^x = (0, h_{ef})^T, \Sigma^x = \begin{pmatrix} \sup \sigma_r^2 & \rho \cdot \sup \sigma_r \cdot \sup \sigma_z & \rho \cdot \sup \sigma_z \cdot \sup \sigma_r \\ \rho \cdot \sup \sigma_r \cdot \sup \sigma_z & \sup \sigma_r^2 & \rho \cdot \sup \sigma_r \cdot \sup \sigma_z \\ \rho \cdot \sup \sigma_z \cdot \sup \sigma_r & \rho \cdot \sup \sigma_r \cdot \sup \sigma_z & \sup \sigma_z^2 \end{pmatrix} \text{correlation } \rho=0, \tag{6.1}$$

The Gaussian “Superpuff” approximation yields the values:  
<sup>sup</sup>σ<sub>r</sub> = 910.1 m; <sup>sup</sup>σ<sub>z</sub> = 412.7 m;  
 DEPL<sub>m=1,...,M</sub>(T<sup>CALM</sup><sub>END</sub>) = 0.915 .... weighted depletion over all pulses - more in Sec. 7

The peripheral distribution of <sup>137</sup>Cs deposition along the circle c\* around the radial beam 69 (drawn in Fig. 6) is demonstrated in Fig. 7. Good fit of both concepts in the central area of interest is evident (better in zoom below). Expected “hard tails” of the non-Gaussian ProcPP can be recognised.

### 7. Comment on prospective assimilation scenarios

The presented scenario incorporates several substantial uncertainties. The most crucial is connected with the estimation of the total radioactivity discharged into the calm region. However, our knowledge of such source terms and their compositions is typically vague and uncertain. Optimal blending of the prior knowledge from the numerical model with real measurements incoming from terrain decreases the degree of uncertainty in our predictions. Various assimilation scenarios can be adjusted in dependence on accessibility of the spatial distribution of the measurement sensors. Let us give a brief outline of the twin experiment when sufficient measurements only in the convective region are available. A proper candidate method for the stepwise recursive re-estimation of the source term and improvement of several input model parameters in the convective region (wind speed, wind direction, release height) could be the nonlinear least-squares regression methodology (e.

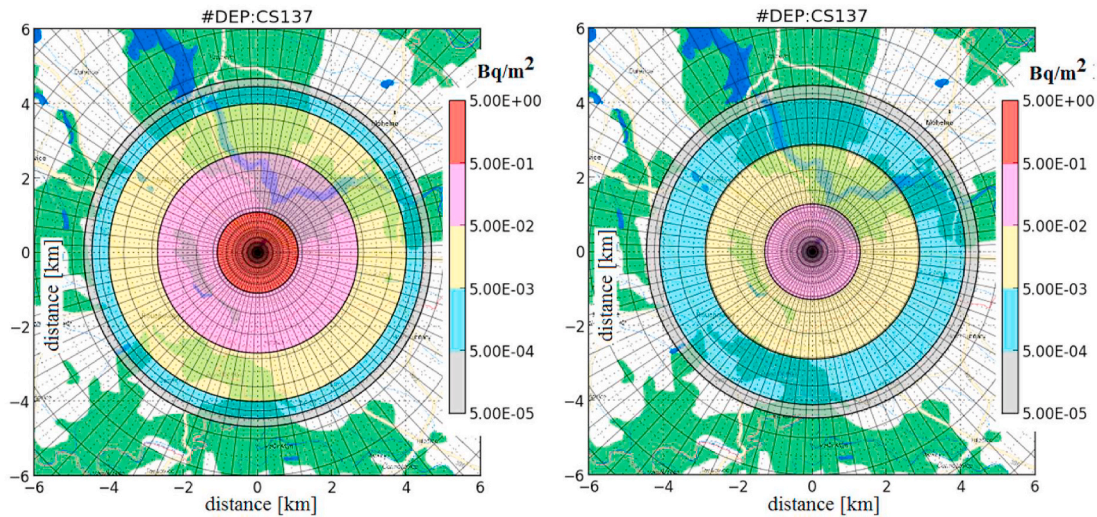


**Fig. 8.** Redistribution of deposited radioactivity of  $^{137}\text{Cs}$  on the ground (deposition in the calm region just at the end of the calm situation at the time  $T_{\text{END}}^{\text{CALM}}$ ) for different values of the gravitational settling velocity. Left:  $vg_{\text{grav}}^n = 0.008 \text{ m}\cdot\text{s}^{-1}$ , Right:  $vg_{\text{grav}}^n = 0.001 \text{ m}\cdot\text{s}^{-1}$ .

g., applied in (Pecha and Šmídl, 2016)). More sophisticated particle filter methods have also been prepared for applications (e.g., (Šmídl and Hofman, 2013)). Principally, the measurements from gamma dose rate (GDR) detectors could be utilized in association with the prior knowledge modelling. The cloud dose rates can be expressed according to the *Case CLOUD* algorithm mentioned in Section 2. Determination of the deposition dose rates are described in detail in Section 3 (for the calm region) and in Section 5 (for the subsequent convective transport).

A substantial benefit could follow from the “*Superpuff*” approach mentioned in Section 4. The results of the statistical pre-processing of the calm distribution are inserted between the calm and convective stages of the trajectory generation. The sum of all discrete pulses (4.1) is substituted by the “*Superpuff*” Gaussian approximation (4.2). It could substantially accelerate the generation of the background trajectories in their convective stages, probably more recognizable for the complex sophisticated dispersion codes. Provided that the discrete pulses  $Q_m^n$ ,  $m \in \{1, \dots, M\}$  are ejected step by step, each until the  $T_{\text{END}}^{\text{CALM}}$  (see Section 3.2), the original total discharged radioactivity is denoted by:

$$Q^{n,\text{TOT}} = \sum_{m=1}^{m=M} Q_m^n \quad (7.1)$$

The radioactivity remaining in the pulse  $m$  at time  $T_{\text{END}}^{\text{CALM}}$  is denoted by  $Q_m^n(T_{\text{END}}^{\text{CALM}})$ . The relationship  $Q_m^n(T_{\text{END}}^{\text{CALM}}) = Q_m^n \cdot \text{DEPL}_m(T_{\text{END}}^{\text{CALM}})$  expresses the depletion of pulse  $m$  on the time interval from its birth until  $T_{\text{END}}^{\text{CALM}}$  (generalised expression (3.3)). The statistical evaluation (Kármý and Guy, 2012) gives Gaussian statistics for the “*Superpuff*” according to Eq. (4.2) together with the weighted depletion  $\text{DEPL}_{m=1,\dots,M}(T_{\text{END}}^{\text{CALM}})$  over all pulses. Similar to (3.2) and terminology in (3.11), the resulting Gaussian “*Superpuff*” related to  $T_{\text{END}}^{\text{CALM}}$  can be approximated as:

$$\text{sup } C^n(T_{\text{END}}^{\text{CALM}}; r, z) = \frac{Q^{n,\text{TOT}} \cdot \text{DEPL}_{m=1,\dots,M}(T_{\text{END}}^{\text{CALM}})^2}{(2\pi)^{3/2} \cdot \text{sup } \sigma_r} \cdot \exp\left(-\frac{r^2}{2 \cdot 2\sigma_r^2}\right) \cdot \Psi(z, \text{sup } \sigma_z, h_{\text{ef}}) \quad (7.2)$$

An important question for the multi-stage *Case CALM* scenario (see Sec. 2) arises from the mapping of the gravitational-settling velocity values. The effect of this parameter is included in the dry deposition parameterization by a combination of Stokes’ law with the Cunningham correction factor for small particles. The importance of the aerosol particle size can be inferred from Fig. 8. The value  $vg_{\text{grav}}^n = 0.008 \text{ m}\cdot\text{s}^{-1}$  has been selected for further calculations (see Section 3.2.2) as an upper

guess. The alternative results have been reached with a decreased value of  $vg_{\text{grav}}^n = 0.001 \text{ m}\cdot\text{s}^{-1}$ . For small aerosol sizes ( $\sim 1.0 \mu\text{m}$ ) we assume this value as the lowest guess. The higher  $vg_{\text{grav}}^n$ , the higher radioactivity remains permanently deposited in the original calm region, and vice versa. Particularly, a poor deposition seen on the right on Fig. 8 implies a higher radioactivity in the cloud entering the surrounding environment in the successive convective stages. The redistribution of the radioactivity between the calm and convective regions is apparent.

## 8. Conclusions

3-D background radiological field simulations are designed for prospective inverse modelling techniques for release of single nuclide  $^{137}\text{Cs}$ . A multi-stage *Case CALM* scenario (see Sec. 2) is proposed. In the first stage, the radioactivity is discharged into the motionless ambient atmosphere. Consecutively, the instant windy conditions replacing the calm meteorological situation drift the “radioactivity reservoir” and cause dissemination of the harmful substances into the environment. The transport of aerosol particles is considered in detail, including the activity depletion mechanisms of radioactive decay, dry activity deposition from the cloud, and radioactivity washout by potential atmospheric precipitation. Each background trajectory of the radioactive pollution consists of two parts relevant to the calm region being altered by a windy transport. An original optional statistical pre-processing of the calm distribution is inserted between the calm and convective stages of the trajectory generation. The pack of accumulated radioactivity in the form of multiple Gaussian puff mixture (sum of all discrete pulses (4.1)) can optionally be substituted into a single representative equivalent Gaussian “*Superpuff*” approximation (4.2). It can substantially accelerate the process of multifold generation of the background trajectories required by the stochastic sampling techniques within the prospective application of the advanced assimilation methods.

Although the probability of a long calm episode is small, its possible consequences can be serious. It is therefore worth examining. The results show a significant increase of deposited radioactivity (especially in combination with rain), which can lead to occurrence of considerable radioactivity hot spots rather far from the release source (Figs. 5 and 6). The code can facilitate the estimation of the results’ sensitivity with respect to the uncertain values of certain essential input parameters (e.g., the gravitational settling - see Fig. 8). Another important application of the presented algorithm is its capability to simulate a continuous release of contamination on the basis of a large number of discrete pulses.

A draft twin experiment is outlined in Section 7 for a simple assimilation scenario for re-estimation of the main model parameters based on a monitoring network in the outer convective region. Basically, the measurements from gamma dose rate (GDR) detectors could be utilized because the corresponding requisite counterpart of the prior knowledge modelling including GDR is available. Cloud dose rates can be expressed according to the *Case CLOUD* algorithm (Section 2). The deposition dose rates are described in detail in Section 3 (for the calm region) and in Section 5 (for the subsequent convective transport).

Development of the model continues for more complex release scenario. Five hours of the calm conditions is immediately succeeded by 4 h of convective transport, all data is extracted from the archived true meteorological measurements. The number of discrete puffs was increased up to  $M = 300$ . Embodiment of more general release source strength shape (constant, serrated, stepwise) is realised – more in (Kárný and Pecha, 2020). Finally, according to authors' experience and strong feeling, the problem of radiological impact of low wind speed dispersion on the living environment should be categorized into the considered conservative weather conditions (worst cases) of the WVA (Weather Variability Assessment) analysis. Compliance of the low wind speed condition consequences with acceptance criteria should always be demonstrated in licensing applications.

### CRedit authorship contribution statement

**Petr Pecha:** Conceptualization, Methodology, Software, Writing - original draft, Validation, Supervision, Writing - review & editing. **Ondřej Tichý:** Visualization, Data curation, Software, Writing - review & editing, Methodology, Validation. **Emilie Pechová:** Project administration, Writing - original draft, Visualization, Writing - review & editing.

### Declaration of competing interest

The authors declare that they have no known competing financial interests or personal relationships that could have appeared to influence the work reported in this paper.

### Acknowledgements

The work of O. Tichý was supported by the Czech Science Foundation, grant no. GA20-27939S. The authors are grateful to the administration of the IT department of the National Radiation Protection Institute in Prague for free access to the archives of the historical meteorological data.

### Appendix A. Supplementary data

Supplementary data related to this article can be found at <https://doi.org/10.1016/j.atmosenv.2020.118105>.

### References

Adriaenssens, S., Cossemans, S., Janssen, L., Mensink, C., 2002. PC-Puff: A Simple Trajectory Model for Local Scale Applications. *Risk Analysis* 22, 915–918.

Anfossi, D., Alessandrini, S., Trini Castelli, S., Ferrero, E., Oetti, D., Degrazia, G., 2006. Tracer dispersion simulation in low wind speed conditions with a new 2D Langevin equation system. *Atmos. Environ.* 40 (2006), 7234–7245.

Baklanov, A., Sorensen, J.H., 2001. Parametrisation of radionuclide deposition in atmospheric long-range transport modelling. *Phys. Chem. Earth* 26 (10).

Carrasi, A., Bocquet, M., Bertino, L., Evensen, G., 2018. Data assimilation in the geosciences: an overview of methods, issues, and perspectives. *Wiley Interdiscipl. Rev.: Clim. Change* 9 (5), e535.

Carruthers, D.J., Weng, W.S., Hunt, J.R.C., Holroyd, R.J., McHugh, C.A., Dyster, S.J., 2003. PLUME/PUFF Spread and Mean Concentration - Module Specifications. ADMS3 Paper P10/01S/03, P12/01S/03.

Deaves, D.M., Lines, J.G., 1998. The nature and frequency of low wind speed conditions. *J. Wind Eng. Ind. Aerod.* 73 (1998).

Drécourt, J.-P., 2004. Data assimilation in hydrological modelling. Environment & Resources DTU. Technical University of Denmark.

EPA, 2004. AERMOD - Description of Model Formulation. U.S. Environmental Protection Agency, Research Triangle Park, NC (Report EPA-454/R-03-004).

Evangelou, N., Hamburger, T., Cozic, A., Balkanski, Y., Stohl, A., 2017. Inverse modeling of the Chernobyl source term using atmospheric concentration and deposition measurements. *Atmos. Chem. Phys.* 17 (14), 8805–8824.

Hanna, R.S., Briggs, G.A., Hosker Jr., R.P., 1982. Handbook on Atmospheric Diffusion. DOE/TIC-11 223, (DE82002045).

HARP, 2010-2019. Environmental SW Package HARP (Hazardous Radioactivity Propagation). <https://havarrp.utia.cas.cz/harp>.

Hofman, R., Pecha, P., 2013. Development of web-based environment for atmospheric dispersion modeling. In: International Topical Meeting on Probabilistic Safety Assessment and Analysis. Columbia, SC, US, 22.09.2013-27.09.2013.

Horst, T.W., 1977. A surface depletion model for deposition from a Gaussian plume. *Atmos. Environ.* 11, 41–46.

Hutchinson, M., Hyondong, O., Wen-Hua, C., 2017. A review of source term estimation methods for atmospheric dispersion events using static or mobile sensors. *Inf. Fusion* 36, 130–148.

Hyojoon, J., Misun, P., Wontae, H., Enuhan, K., Moonhee, H., 2013. The effect of calm conditions and wind intervals in low wind speed on atmospheric dispersion factors. *Ann. Nucl. Energy* 55 (2013), 230–237.

International Atomic Energy Agency (IAEA), 2011. Source of Iodine-131 in Europe Identified. <https://www.iaea.org/newscenter/pressreleases/source-iodine-131-europe-identified>. Oct. 2011.

Jones, J.A., 1996. Atmospheric Dispersion at Low Wind Speed. Liaison Comm. Annual Report, 1996-1997, ANNEX A, NRPB-R292.

Kabanikhin, S.I., 2008. Definitions and examples of inverse and ill-posed problems. *J. Inverse Ill-Posed Probl.* 16 (2008), 317–357.

Kárný, M., Guy, T.V., 2012. On Support of imperfect bayesian participants. *Decis. Making Imperfect Decis. Makers* 29–56. [https://doi.org/10.1007/978-3-642-24647-0\\_2](https://doi.org/10.1007/978-3-642-24647-0_2).

Kárný, M., Pecha, P., 2020. Flexible Modelling of Radioactive Release into the Motionless Atmosphere: A Multiple Pulse Approach. Submitted for publication.

Korsakissok, I., Andronopoulos, S., Astrup, P., Bedwell, P., Chevalier-Jabet, K., de Vries, H., Geertsema, G., Gering, F., Hamburger, T., Klein, H., Leadbatter, S., Mathieu, A., Pázmándi, T., Périllat, R., Rudas, C., Sogachev, A., Szanto, P., Tomas, J., Twenhöfel, C., Wellings, J., 2020. Comparison of ensembles of atmospheric dispersion simulations: lessons learnt from the confidence project about uncertainty quantification. In: 19th International Conference on Harmonisation within Atmospheric Dispersion Modelling for Regulatory Purposes.

Kovalets, I., Andropoulos, S., Hofman, R., Siebert, P., Ievdin, I., 2016. Advanced method for source estimation and status of its integration in JRODOS. *Radioprotection* 51 (HS2), 121–123.

Lines, J.G., Deaves, D.M., 1997. The Implication in Dispersion in Low Wind Speed Condition for Qualified Risk Assessment. WS Atkins Consult., WSA/RSU 8000/035.

Lines, J.G., Daycock, J.H., Deaves, D.M., 2001. Guidelines for the inclusion of low wind speed conditions into risk assessment. *J. Hazard Mater.* 2001 (May 30), 153–179.

McGuire, S.A., Ramsdell, J.V., Athey, G.F., 2007. RASCAL 3.0.5: Description of Models and Methods. NUREG – 1887.

NRPB-R302, 1999. Atmospheric Dispersion Modelling. Liaison Committee Annual Report 1996/1997.

Okamoto, S., Onishi, H., Yamada, T., Mikami, T., Momose, S., Shinji, H., Itoha, T., 2001. A model for simulating atmospheric dispersion in a low wind condition. *Int. J. Environ. Pollut.* 16 (2001).

Pandey, G., Sharan, M., 2019. Accountability of wind variability in AERMOD for computing concentrations in low wind conditions. *Atmos. Environ.* 202 (2019), 105–116.

Pecha, P., Pechová, E., 2014. An unconventional adaptation of a classical Gaussian plume dispersion scheme for the fast assessment of external irradiation from a radioactive cloud. *Atmos. Environ.* 89 (6), 298–308, 2014.

Pecha, P., Šmíd, V., 2016. Inverse modelling for real-time estimation of radiological consequences in the early stage of an accidental radioactivity release. *J. Environ. Radioact.* 164 (1), 377–394, 2016.

Pecha, P., Hofman, R., Václav, Šmíd, 2009. Bayesian Tracking of the Toxic Plume Spreading in the Early Stage of Radiation Accident. *ESM'2009. European Simulation and Modelling Conference*, Leicester, GB, pp. 381–387, 26.10.2009–29.10.2009.

Pecha, P., Tichý, O., Pechová, E., 2020. Potential Radioactive Hot Spots Induced by Radiation Accident Being Underway of Atypical Low Wind Meteorological Episodes. *Inst. of Information Theory and Automation, Praha, CZ. Research Report 2382*.

Pöllänen, R., Toivonen, H., Lahtine, J., Ilander, T., 1995. Transport of Large Particles Released in a Nuclear Accident. STUK-A125. OCTOBER 1995.

Rakesh, P.T., Venkatesan, R., Srinivas, C.V., Baskaran, R., Venkatraman, B., 2019. Performance evaluation of modified Gaussian and Lagrangian models under low wind speed: a case study. *Ann. Nucl. Energy* 133, 562–567, 2019.

Saunier, O., Mathieu, A., Didier, D., Tombette, M., Quélo, D., Winiarek, V., Bocquet, M., 2013. Using gamma dose rate monitoring with inverse modelling techniques to estimate the atmospheric release of a nuclear power plant accident: application to the Fukushima case. In: Proceedings of the 15th Conference on "Harmonisation within Atmospheric Dispersion Modelling for Regulatory Purposes", Madrid, Spain, May 6–9, 2013.

Saunier, O., Didier, D., Mathieu, A., Masson, O., Brazidec, J., 2019. Atmospheric modeling and source reconstruction of radioactive ruthenium from an undeclared major release in. *Proc. Natl. Acad. Sci. Unit. States Am.* 116 (50), 201907823, 2017.

- Schichtel, T., 2019. Description of the Source Term Reconstruction Model SSTR in RODOS. Karlsruhe Ins. Of Tech., Version 1.0 (JRODOS 2019).
- Šmídl, V., Hofman, R., 2013. Adaptive importance sampling in particle filtering. In: *Proceeding of the 16th International Conference on Information Fusion, (Istanbul, TR, 09.07.2013-12.07.2013)*.
- Šmídl, V., Hofman, R., 2013a. Tracking of atmospheric release of pollution using unmanned aerial vehicles. *Atmos. Environ.* 67 (1), 425–436, 2013.
- Šmídl, V., Pecha, P., Hofman, R., 2013. Data Assimilation Methods Used in the ASIM Module - Draft Version. UTIA Report No. 2333.
- Šmídl, V., Pecha, P., Hofman, R., 2014. Evaluation of detection abilities of monitoring networks using multiple assessment criteria. *Int. J. Environ. Pollut.* 129–138.
- Sportisse, B., 2007. A review of parameterization for modelling dry deposition and scavenging of radionuclides. *Atmos. Environ.* 41 (2007), 2683–2698.
- Stohl, A., Seibert, P., Wotawa, G., Arnold, D., Burkhardt, J.F., Eckhardt, S., Tapia, C., Vargas, A., Yasunari, T.J., 2012. Xenon-133 and caesium-137 releases into the atmosphere from the Fukushima Dai-ichi nuclear power plant: determination of the source term, atmospheric dispersion, and deposition. *Atmos. Chem. Phys.* 12, 2313–2343. <https://doi.org/10.5194/acp-12-2313-2012>.
- Tichý, O., Šmídl, V., Hofman, R., Stoh, A., 2016. LS-APC v1.0: a tuning-free method for the linear inverse problem and its application to source-term determination. *Geosci. Model Dev. (GMD)* 9, 4297–4311.
- Tichý, O., Šmídl, V., Hofman, R., Šindelářová, K., Hýža, M., Stohl, A., 2017. Bayesian inverse modelling and source location of an unintended 131I release in Europe in the fall of 2011. *Atmos. Chem. Phys.* 17, 12677–123696, 2017.
- Tichý, O., Šmídl, V., Hofman, R., Evangelidou, N., 2018. Source term estimation of multi-species atmospheric release of radiation from gamma dose rates. *Q. J. R. Meteorol. Soc.* 144 (717), 2781–2797.
- Tichý, O., Šmídl, V., Hýža, M., 2019. Bayesian approach to localization of atmospheric release with demonstration on the case of ruthenium-106 release in 2017. In: *SnT 2019 - CTBT: Science and Technology Conference - Book of Abstracts*, p. 175. Vienna, AT.
- Tsuda, A., Henry, F.S., Butler, J.P., 2013. Particle transport and deposition: basic physics of particle kinetics. *Comp. Physiol.* 3 (4), 1437–1471.
- Winiarek, V., Bocquet, M., Duhanyan, N., Roustan, Y., Saunier, O., Mathieu, A., 2014. Estimation of the caesium-137 source term from the Fukushima Daiichi nuclear power plant using a consistent joint assimilation of air concentration and deposition observations. *Atmos. Environ.* 82, 268–279, 2014.
- Zannetti, P., 1990. *Air Pollution Modeling. Theories, Computational Methods and Available Software*, 1 – 85312-100-2.

### Further reading

- Hofman, R., Pecha, P., Šmídl, V., 2013. Distributed Framework for Modeling and Reconstruction of Nuclear Accidents, 63-63. *Book of Abstracts of CTBT Science and Technology 2013 Conference, Vienna, AT, 17.-21.6. 2013.*